Aalto University

Aaltodoc
OPEN ACCESS

This is an electronic reprint of the original article.
This reprint may differ from the original in pagination and typographic detail.

Author(s): Foster, A. S. & Lopez Gejo, F. & Shluger, A. L. & Nieminen, Risto M.

Title: Vacancy and interstitial defects in hafnia

Year: 2002

Version: Final published version

Please cite the original version:

Foster, A. S. & Lopez Gejo, F. & Shluger, A. L. & Nieminen, Risto M. 2002. Vacancy and interstitial defects in hafnia. Physical Review B. Volume 65, Issue 17. 174117/1-13. ISSN 1550-235X (electronic). DOI: 10.1103/physrevb.65.174117.

Rights: © 2002 American Physical Society (APS). This is the accepted version of the following article: Foster, A. S. & Lopez Gejo, F. & Shluger, A. L. & Nieminen, Risto M. 2002. Vacancy and interstitial defects in hafnia. Physical Review B. Volume 65, Issue 17. 174117/1-13. ISSN 1550-235X (electronic). DOI: 10.1103/physrevb.65.174117, which has been published in final form at http://journals.aps.org/prb/abstract/10.1103/PhysRevB.65.174117.

All material supplied via Aaltodoc is protected by copyright and other intellectual property rights, and duplication or sale of all or part of any of the repository collections is not permitted, except that material may be duplicated by you for your research use or educational purposes in electronic or print form. You must obtain permission for any other use. Electronic or print copies may not be offered, whether for sale or otherwise to anyone who is not an authorised user.

Vacancy and interstitial defects in hafnia

A. S. Foster,[1] F. Lopez Gejo,[2] A. L. Shluger,[2] and R. M. Nieminen[1]

[1]*Laboratory of Physics, Helsinki University of Technology, P.O. Box 1100, FIN-02015, Finland*

[2]*Department of Physics and Astronomy, University College London, Gower Street, London WC1E 6BT, United Kingdom*

(Received 20 December 2001; revised manuscript received 4 March 2002; published 2 May 2002)

We have performed plane wave density functional theory calculations of atomic and molecular interstitial defects and oxygen vacancies in monoclinic hafnia (HfO_2). The atomic structures of singly and doubly positively charged oxygen vacancies, and singly and doubly negatively charged interstitial oxygen atoms and molecules are investigated. We also consider hafnium vacancies, substitutional zirconium, and an oxygen vacancy paired with substitutional zirconium in hafnia. Our results predict that atomic oxygen incorporation is energetically favored over molecular incorporation, and that charged defect species are more stable than neutral species when electrons are available from the hafnia conduction band. The calculated positions of defect levels with respect to the bottom of the silicon conduction band demonstrate that interstitial oxygen atoms and molecules and positively charged oxygen vacancies can trap electrons from silicon.

DOI: 10.1103/PhysRevB.65.174117 PACS number(s): 61.72.−y, 71.20.−b, 85.50.−n, 77.84.−s

I. INTRODUCTION

Hafnia (HfO_2) is a hard material with a relatively high dielectric constant and wide band gap.[1–3] It also has high thermal stability and is used in optical and protective coatings.[1,4] However, the basic properties of hafnia (HfO_2) have been little studied in the literature, with only a scattering of experimental and theoretical works. Due to their homological outer shell electronic configuration,[5,6] its properties are expected to be similar to zirconia. In particular, hafnia also exists in three polymorphs at atmospheric pressure: at low temperatures the monoclinic C_{2h}^5 phase (space group $P2_1/c$), above 2000 K the tetragonal D_{4h}^{15} ($P4_2/nmc$) phase, and above 2870 K the cubic fluorite O_h^5 ($Fm3m$) phase. Although there are some experimental studies of the monoclinic phase,[2,6–8] there are very few studies of the tetragonal or cubic phases.[1] Also experimental and theoretical studies of the structure and properties of point defects in hafnia are, to our knowledge, absent.

Along with several other high-dielectric-constant materials,[9] hafnia-related research is increasing rapidly due to its potential for substituting silicon dioxide in its role as gate dielectric in microelectronic devices. Thin HfO_2 films grown on silicon demonstrate favorable parameters, such as high thermal stability and low leakage current.[10–12] The structure and composition of such films grown, for example, using atomic layer deposition on silicon,[4,13] chemical solution deposition on silicon dioxide,[14] and other methods,[12,15] have been characterized by transmission electron microscopy, x-ray diffraction, reflection high-energy electron diffraction (HREED), and electron microprobe analysis.[2] It was found that after annealing in oxygen at 500–1200 °C crystalline films are almost always nearly stoichiometric monoclinic HfO_2.

The performance of thin hafnia films as gate dielectrics is likely to be affected by various lattice defects. In particular, film annealing involves oxygen diffusion through the already grown oxide and the possible formation of interstitial oxygen. Experiments on zirconia[16–18] have suggested that oxygen incorporates from the surface and diffuses inside the oxide in atomic form. Since such experiments are still absent for hafnia, it is interesting to use theory to determine the most stable forms of interstitial oxygen species in this material. Another important issue is related to oxygen stoichiometry and formation of oxygen vacancies. As-grown films are almost always nonstoichiometric, although this can be corrected by high-temperature annealing. However, the concentration of remaining oxygen vacancies is unclear. Electron and hole trapping by interstitial oxygen and oxygen vacancies may affect leakage current through the oxide. For example, recent studies of plasma-deposited zirconia thin films on silicon[19] have demonstrated significant electron and hole trapping, and this is supported by theoretical predictions of the trapping properties of vacancies and interstitials in zirconia.[20] Charged defects can create strong electric fields and affect band offsets. They can contribute to dielectric loss and their diffusion in an electric field is equivalent to electrolysis (see, for example, Ref. 21). These issues are critical to the performance of thin hafnia films and have yet to be studied. The structure and properties of oxygen vacancies and interstitial oxygen atoms have recently been studied in zirconia[20,22,23] and zircon ($ZrSiO_4$).[24]

In this paper we use density functional theory (DFT) calculations to study the structure and electronic properties of three stable phases of crystalline hafnia, and of oxygen vacancy and interstitial defects in monoclinic hafnia. We consider stable configurations of neutral oxygen vacancies and interstitial oxygen atoms and molecules in the bulk of this material. As in the case of Si/SiO_2,[25] the charge state of these defects in a hafnia film on silicon can be changed by electron transfer from/to the silicon substrate. Therefore we calculate the electron and hole affinities of these defects and study their stable configurations in different charge states. The obtained defect properties allow us to calculate the energies of various defect processes involving these defects. The results demonstrate that interstitial oxygen atoms and positively charged oxygen vacancies can trap electrons from the bottom of the hafnia conduction band and from silicon.

The paper is organized as follows. In the next section we

 ©2002 The American Physical Society

TABLE I. Comparison of calculated and experimental (Refs. 32 and 33) properties of bulk hcp hafnium.

Property	Calc.	Expt.
a (Å)	3.1797	3.1946
c (Å)	5.0239	5.0510
c/a	1.58	1.58
V_0 (Å^3)	21.99	22.32
B_0 (GPa)	110	110

discuss the details and justification of the methods of calculation. In the third section we discuss the results for the two classes of point defects, interstitials and vacancies, and then in the fourth section we study the reactions between defects. Finally, we summarize the implications and possible future directions of the study.

II. METHOD

A. Ideal crystals

All the calculations have been performed using the plane wave basis VASP code,[26,27] implementing spin-polarized DFT and the generalized gradient approximation (GGA) of Perdew and Wang[28] known as GGA-II. We have used ultrasoft Vanderbilt pseudopotentials[29,30] to represent the core electrons. The pseudopotential for the hafnium atom was generated in the electron configuration $[\mathrm{Xe}\,4f^{14}]5d^{3}6s^{1}$ and that for the oxygen atom in $[1s^{2}]2s^{2}2p^{4}$, where the core electron configurations are shown in square brackets.

In order to validate both the pseudopotentials and the method itself, and to find the chemical potential of Hf, extensive calculations were performed on bulk hcp hafnium and the three dominant bulk phases of hafnia: cubic, tetragonal, and monoclinic. For the pure metal, the total energy was found to converge to within 10 meV for a plane wave cutoff energy of 250 eV and 252 k points in the irreducible part of the Brillouin zone (BZ). The bulk unit cell lattice vectors and atomic coordinates were then relaxed at a series of fixed volumes. The obtained energies were fitted with a Murnaghan equation of state[31] to give the equilibrium volume and the minimum energy. The final calculated cell parameters are given in Table I, along with experimental values.

For hafnium oxide, total energy convergence was tested for each phase within a BZ sampling range between 1 and 80 k points and a plane wave cutoff energy range between 200 and 700 eV. Convergence to within 10 meV was achieved with 20 k points and a cutoff energy of 400 eV. The bulk unit cell lattice vectors and atomic coordinates were then relaxed and fitted as for calculations of hafnium. The final calculated cell parameters are given in Table II, along with experimental values.

For both pure hafnium and the hafnia phases, we have found good agreement between calculated and available experimental values of structural parameters of these systems. Our results are also in good agreement with previous DFT calculations of this material.[35] Note however, that the experimental data for cubic and tetragonal phases are taken at high temperature, e.g., 2073 K for tetragonal, and are also somewhat dependent on temperature, and therefore comparisons with the 0 K theoretical data are limited.

TABLE II. Comparison of calculated and experimental (Refs. 1,7, and 34) bulk unit cell parameters for the cubic, tetragonal, and monoclinic phases of hafnia. δz is the shift in fractional coordinates of oxygen atoms in the tetragonal cell with respect to their ideal cubic positions, β is the angle between lattice vectors a and c in the monoclinic cell, and and x,y,z are the fractional coordinates of the nonequivalent sites in the m structure.

Property	Calculated	Experimental
Volume (Å^3)	32.49	32.77
a (Å)	5.07	5.08
	Tetragonal	
Volume (Å^3)	33.12	35.075
a (Å)	5.06	5.15
c/a	1.024	1.027
δz	0.051	-
	Monoclinic	
Volume (Å^3)	34.81	34.62
a (Å)	5.1322	5.1187
b/a	1.011	1.010
c/a	1.034	1.035
β (deg)	99.78	99.18
Hf_x	0.277	0.276
Hf_y	0.044	0.040
Hf_z	0.209	0.207
$\mathrm{O1}_x$	0.070	0.071
$\mathrm{O1}_y$	0.333	0.332
$\mathrm{O1}_z$	0.345	0.344
$\mathrm{O2}_x$	0.448	0.446
$\mathrm{O2}_y$	0.758	0.755
$\mathrm{O2}_z$	0.478	0.480
	Energy differences between phases (/HfO_2)	
E^{t-c} (eV)	-0.08	-
E^{m-c} (eV)	-0.24	-

The electron density of states (DOS) for ideal monoclinic hafnia is shown in Fig. 1(a). For better presentation, each of the discrete one-electron energies forming the spectrum was broadened by a Gaussian with a smearing factor equal to 0.3 eV. Note that tails at the band edges are determined by this factor and do not have a quantitative meaning, but the raw DOS at the valence band edge can be seen in Fig. 1(b). The DOS for the monoclinic phase is very similar to the DOS obtained for the cubic and tetragonal phases (not shown here) and has three clear bands. A valence band of oxygen $2s$ character at around -15 eV, a valence band of oxygen $2p$ character at around 0 eV and a conduction band of hafnium $5d$ character at around 7 eV. There is a small number of states of Hf $5d$ character in the middle band, but it is dominated by the O $2p$ states. This is consistent with the picture of hafnia as an ionic insulator, with some degree of covalent bonding between Hf and O. The fact that the top of the

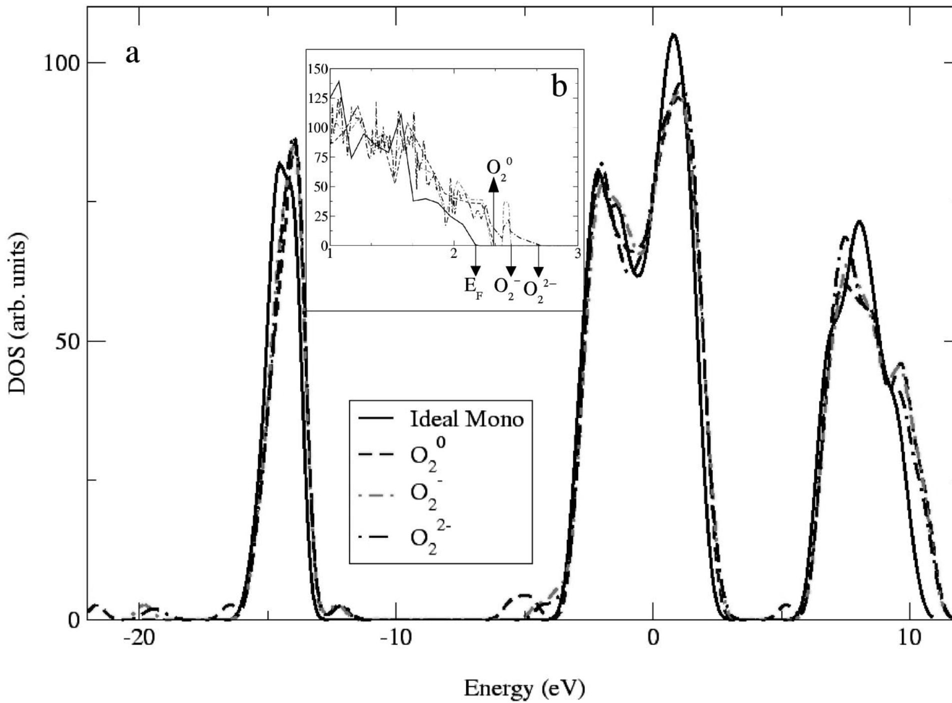

FIG. 1. (a) Total density of states (DOS) for ideal and defected monoclinic hafnia. Note that Gaussian smearing has been applied to the DOS for clarity. (b) An enlargement of the unsmeared DOS around the Fermi level (E_F) of the ideal system, at 2.1 eV. The arrows show the highest occupied one-electron states of the defected systems, O_2^0 at 2.25 eV, O_2^- at 2.40 eV, and O_2^{2-} at 2.70 eV.

Kohn-Sham O $2p$ valence band states is located at about 2.1 eV is an artifact of the calculation procedure.

The band gap calculated as the energy difference between the highest occupied and lowest unoccupied one-electron states in this method is 4.12 eV. Using a method described previously,[20] the band gap estimated as a difference of the total energies of the system with N, $N+1$, and $N-1$ electrons is 3.92 eV. The gap values obtained using both methods are much smaller than the experimental value of 5.68 eV.[2] Note that the band gap in hafnia is larger than the corresponding value of 3.19 eV obtained in zirconia by the same method,[20] and is consistent with the smaller experimental value of 5.4 eV in zirconia.[23]

B. Calculation of defect properties

All defect calculations were made using a 96 atom unit cell, which is generated by extending the 12 atom monoclinic unit cell by two in three dimensions. The monoclinic structure is used in calculations since it is the most stable phase, even for thin films.[2,13,14]

For this cell, the total energy was converged to better than 40 meV for a plane wave cutoff of 500 eV and 2 k points in the first BZ. One oxygen atom/molecule was added to or extracted from this cell to model the interstitial and vacancy defects, respectively. A neutralizing background was applied to the unit cell for calculations of charged defects. The large size of the cell separates the periodic defect images by over 10 Å. The Coulomb interaction between charged defects in different periodic cells calculated as described in Refs. 36 and 37 and using a Madelung constant calculated in VASP in most cases does not exceed 0.1 eV.

The perturbation of the DFT effective potential caused by the introduction of defects to the cell can be seen in Fig. 1(a) for the molecular interstitials (slightly smaller shifts are seen in the atomic interstitial DOS). The band edges shift by about 0.1 eV from the ideal bulk position upon introduction of a neutral molecule, but there is little difference in the Fermi level position for different defect charge states. This confirms the fact that the artificial Coulomb interaction between charged defects is very small. For geometry relaxation we used a combination of conjugate gradient energy minimization and quasi-Newton force minimization. During defect calculations the lattice vectors of the cell were frozen, which corresponds to a very dilute system. All atoms were allowed to relax until atomic forces were less than 0.05 eV/Å.

The vacancy formation energies (or equivalently, the oxygen atom/molecule incorporation energies) $E_{\rm for}(D)$ were calculated as the energy difference between the fully relaxed defected neutral supercell, E_D^0, and the perfect neutral monoclinic 96 atom unit cell, E_0^0, and an isolated oxygen atom/molecule, E_O, according to

$$E_{\rm for}(D)=E_D^0-(E_0^0\pm E_{\rm O}). \qquad (1)$$

Here $E_{\rm O}$ is the total energy of the individual oxygen atom or molecule. It is subtracted for a vacancy and added for an interstitial. Calculation of $E_{\rm O}$ is discussed in detail below.

In order to study stable charged defect states and the possible role of defects in photo- and thermostimulated processes, and in electronic devices one needs to know electron affinities and ionization energies of defect states with respect to the bottom of the conduction band of hafnia and to other electron or hole sources, such as silicon. To achieve that, we compare total energies of the initial and final systems with the same number of electrons. The main inaccuracy of this approach is related to the underestimated band gap in DFT calculations (see also the discussion in Ref. 20). This means that defect states are closer than they should be to the top of the valence band and the bottom of hafnia conduction band.

The relative error with respect to the gap edges depends on a defect and is impossible to establish without proper calibration using experimental data.

Defining the absolute value of the defect ionization energy $I_p(D^q)$ as the vertical excitation energy of an electron from the defect with charge q to the bottom of the conduction band, we have

$$I_p(D^q)=E_0^- + E_D^{q+1} - E_0^0 - E_D^q + \kappa_1, \qquad (2)$$

where E_0^- and E_0^0 are the calculated energies of the perfect supercell with charge -1 and 0, respectively, and E_D^q is the energy of the defect with the charge q (in the elementary charge unit). In Eq. (2) the value E_D^{q+1} is calculated for the geometry of the relaxed defect with charge q and κ_1 is a correction for the position of the bottom of the conduction band. Similarly we can define the electron affinity of the defect $\chi_e(D^q)$ (i.e., the energy gain when the electron from the bottom of the conduction band is trapped at the defect) as follows:

$$\chi_e(D^q)=E_0^- + E_D^q - E_0^0 - E_D^{q-1} + \kappa_2. \qquad (3)$$

Here the correction κ_2 can be generally different from κ_1. One can consider both "vertical" and "relaxed" electron affinities. In the latter case the lattice relaxation after the electron trapping is included in E_D^{q-1}. We can also define the hole affinity of the defect $\chi_h(D^q)$, i.e., the energy gain when the a free hole is trapped from the top of the valence band to the defect as follows:

$$\chi_h(D^q)=E_0^+ + E_D^q - E_0^0 - E_D^{q+1} + \kappa_3. \qquad (4)$$

Again, dependent on whether the lattice relaxation in the final state is included or not, one will obtain different affinities. The vertical hole affinity provides a useful estimate of the position of the defect state with respect to the top of the valence band. To define the corrections κ_1, κ_2, κ_3 we use the following considerations. (i) We assume that the main inaccuracy in defining the relative positions of defect states with respect to the band-gap edges is due to unoccupied Kohn-Sham states, and that the underestimated band gap is mainly due to the too low position of the bottom of the conduction band. Therefore we use an approximation that $\kappa_1=\kappa_2=\kappa$ and $\kappa_3=0$. These conditions are difficult to fully justify without comparison with experiment. As we will show below, the vertical hole affinities calculated as the difference between one-electron states and using Eq. (4) agree within 0.5 eV, which gives an indication of an error made by this assumption. (ii) Using these conditions and definitions (3) and (4) it is easy to obtain

$$\chi_h(D^q)+\chi_e(D^{q+1})=E_g(\text{expt}), \qquad (5)$$

where both affinities correspond to relaxed final defect states. This condition holds in all calculations, which ensures the consistency of our approach. (iii) We use the experimental value of $E_g(\text{expt})=5.68$ eV (Ref. 2) to define the difference

$$\kappa=E_g(\text{expt})-E_g(\text{theor}), \qquad (6)$$

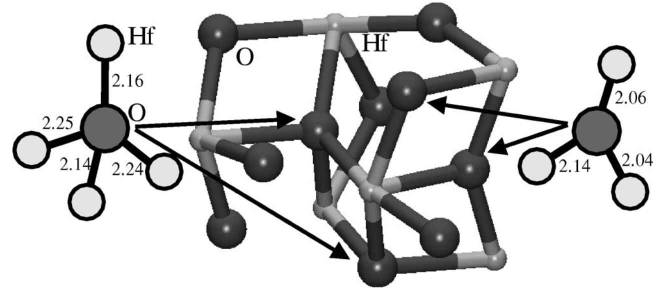

FIG. 2. Diagram showing the fourfold-coordinated tetragonal (left) and threefold-coordinated trigonal (right) bonding of the oxygen ions in the monoclinic phase of hafnia as calculated in this work. The numbers show interatomic distances in Å.

and correct the defect excitation energies, the ionizational potentials, and electron affinities. This gives $\kappa=5.68-3.92=1.76$ eV, which is used in all further calculations.

Although this method is approximate, fixing the value of κ allows us to present the results of our calculations in one scale. Another advantage is that, in order to find defect affinities with respect to electrons at the bottom of silicon conduction band or holes at the top of the silicon valence band, within the same method one can use the experimental value of the band offset with Si. This scale can be changed if a more "accurate" or relevant value for κ will be found. This will require only a shift of our predicted values by a constant.

III. INCORPORATION OF ATOMIC OXYGEN

Unlike for silica and zirconia, incorporation of oxygen species in hafnia has been studied neither experimentally nor theoretically. In view of the potential applications of hafnia as a gate oxide, development of structural models of oxygen species in this material and comparison with other systems seems partcularly timely. Defect species in gate oxides can be charged by electrons or holes tunneling from Si. Therefore in this study we have first considered interstitial neutral oxygen atom and then studied the possibility of formation and equilibrium structures of charged species $X=O^-$ and O^{2-}. As discussed below, each interstitial can form a stable defect at either a fourfold-coordinated tetragonally or threefold-coordinated trigonally bonded lattice oxygen site (see Fig. 2). For ease of reference all values associated with a threefold-coordinated oxygen will be labeled X_3 and all associated with a fourfold-coordinated oxygen will be labeled X_4, where X is the defect species.

A. Incorporation energies

The incorporation energy of atomic oxygen into the hafnia lattice can be calculated with respect to different processes involving gas oxygen species. For example, molecular oxygen participates in high-temperature annealing of films.[11–14] In this case an oxygen molecule in the lowest triplet state provides the right reference for the chemical potential (see discussion in Ref. 24). This approach has been used in many similar studies (see, for example, Refs.

20,24,38 and 39). Using half of the energy of an isolated O_2 molecule (equal in our VASP calculations to 4.91 eV) as a reference energy, E_O [see Eq. (1)], we obtain defect formation energies $+1.6$ eV for O_3^0 and $+2.3$ eV for O_4^0. A positive value indicates an endothermic process, which involves dissociation of the O_2 molecule.

In the ultraviolet ozone oxidation process (see, for example, Ref. 40), ultraviolet light interacts with oxygen gas to produce oxygen radicals and ozone. To estimate whether the incorporation from atomic gas is exothermic, one should know the energy of an oxygen atom in the triplet state. This is known to be a problem in plane wave DFT as the result depends on the shape of the unit cell. Using a series of expanding rectangular periodic cells with three different lattice constants exceeding 10 Å, we obtained a "broken symmetry" solution for the oxygen atom with a lowest energy $E_O = -1.97$ eV. This then gives the dissociation energy of the O_2 molecule in GGA-II as 5.88 eV, which is higher than the experimental value of 5.17 eV.[33] The electron affinity of the oxygen atom calculated using the same approach is 1.7 eV, slightly higher than the experimental value of 1.5 eV.[33]

Using atomic E_O as a reference, we find formation energies for single O atom incorporation into the monoclinic hafnia lattice of -1.3 eV (O_3^0) and -0.6 eV (O_4^0). These values are close to those found for oxygen incorporation in zirconia [-1.6 eV (O_3^0) and -0.8 eV (O_4^0) (Ref. 20)] and zircon [-1.2 eV (Ref. 24)]. They can be also compared with values reported in the literature for the same process in α-quartz. Using a plane wave LDA approach Hamann has found a formation energy of -0.86 eV;[41] a similar value, -0.7 eV has been reported from correlated cluster calculations[42] and -0.9 eV in recent DFT GGA-II calculations.[43]

Since the O_3^0 site is energetically favored, the rest of this discussion will focus only on this site. Note also that previous studies in zirconia have shown that there is no stable minimum for charged defects at the O_4 sites.[20]

B. Defect models and electron affinities

For the neutral interstitial, a charge density map in Fig. 3 shows that the oxygen defect forms a clear covalent bond with the threefold-coordinated lattice oxygen. The interstitial and lattice oxygen form a "dumbbell" defect pair structure, which is characteristic of other oxides, such as zirconia[20] and zircon ($ZrSiO_4$).[24] To accommodate the interstitial, the lattice oxygen displaces from its planar position between three Hf ions to form a shallow pyramid. In this structure the two oxygens are effectively identical structurally and electronically, although small differences in bond lengths evidence slightly different environments, and the interstitial is bound to only two of the three hafnium ions in the pyramid. The interstitial incorporates in the lowest singlet state—the triplet state is 0.9 eV higher in energy.

To study an electron trapping by the defect, an extra electron was added into the system in the atomic configuration of the neutral interstitial. The electron does not initially localize at the defect site, but rather remains delocalized with its energy very close to the bottom of the conduction band. Therefore the vertical electron affinity is close to zero. We should note that this can be an artifact of our DFT calculation caused by the wrong position of the bottom of the conduction band and by the well-known tendency of DFT to underestimate the degree of localization of electron states in shallow traps.[44–46]

FIG. 3. Charge density in the plane through Hf_A, O_A, and O_i, and a schematic diagram of neutral oxygen interstitial (O_i) near a threefold-coordinated oxygen (O_A) in hafnia. The charge density is in $0.1e/Å^3$ and all distances are in Å.

System relaxation leads, however, to complete localization of the electron on the oxygen pair. The increased charge on the defect oxygen pair causes the ions to separate, also increasing the depth of the triple oxygen pyramid. Figure 4 demonstrates that the covalent bond between the two has almost disappeared, although they remain effectively still a similar species within the crystal. The relaxation energy from the initial O_3^0 configuration is equal to 2.3 eV. The electron is fully localized in a doublet state on the defect pair. The calculated relaxed electron affinity of the neutral interstitial oxygen atom in the O_3^0 configuration with respect to the electron at the bottom of the hafnia conduction band is given in Table III. Note that in our notations positive affinity means that an electron prefers to be on the defect, rather than at the bottom of the conduction band.

Addition of the second electron from the conduction band to the negatively charged defect is again accompanied by strong lattice relaxation. As in the case of the singly charged defect, the vertical electron affinity is close to zero and the relaxed affinity is positive (see Table III). Introduction of the second electron effectively produces two independent lattice oxygen ions. The separation between them increases even further, to about 2.4 Å, and Fig. 5 clearly shows that there is no bond between the two oxygen ions. The corresponding

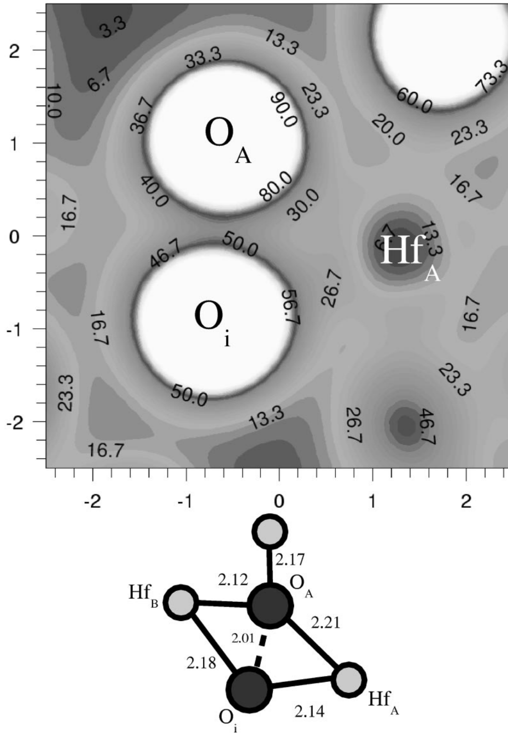

FIG. 4. Charge density in the plane through Hf_A, O_A, and O_i, and schematic diagram of the singly charged oxygen interstitial (O_i) near a threefold-coordinated oxygen (O_A) in hafnia. The charge density is in $0.1e/Å^3$ and all distances are in Å.

relaxation energy is about 1.53 eV. The original threefold-coordinated lattice oxygen is pushed into a deeper pyramid structure with the three Hf ions, but the interstitial now creates a new threefold-coordinated site, bonding with a third, independent, hafnium ion at 2.2 Å. In the previous defect structures, this hafnium ion was over 2.6 Å from the interstitial (and over 4 Å from the lattice oxygen) and no bond could be seen in the charge density. The new electron is fully localized on the defect oxygen pair, which is in the singlet state with equal spin components.

TABLE III. Ionizational potential $I_p(D)$, relaxed electron $\chi_e(D)$, and hole $\chi_h(D)$ affinities (in eV) of defects in different charge states.

D	$I_p(D)$	$\chi_e(D)$	$\chi_h(D)$
V_4^0	3.88	-	2.42
V_4^+	4.10	3.27	2.42
V_4^{2+}	-	3.26	-
V_3^0	3.41	-	2.92
V_3^+	3.75	2.76	2.75
V_3^{2+}	-	2.93	-
O_3^0	5.55	3.95	0.19
O_3^-	5.38	4.75	1.73
O_3^{2-}	5.35	-	0.92
$(O_2^0)_3$	5.53	4.67	0.20
$(O_2^-)_3$	5.46	5.06	1.01
$(O_2^{2-})_3$	5.32	-	0.62
$(V_3+S_{Zr})^0$	3.46	2.03	2.82
$(V_3+S_{Zr})^+$	3.86	2.86	2.63
$(V_3+S_{Zr})^{2+}$	-	3.05	-

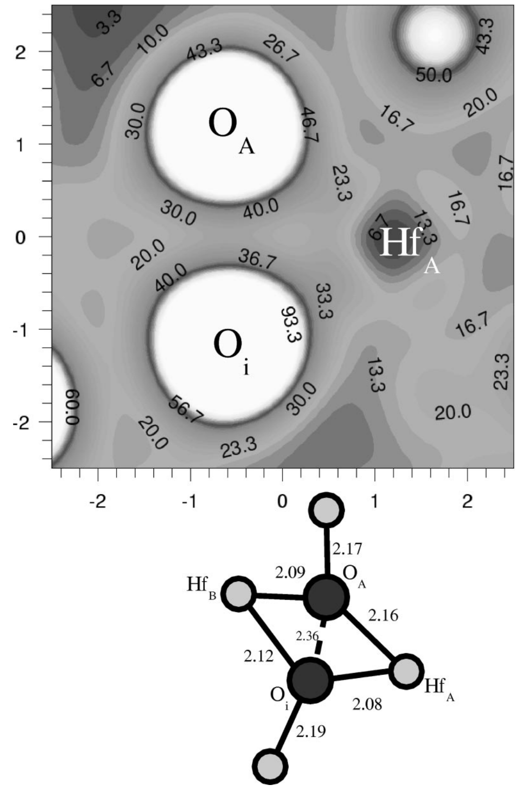

FIG. 5. Charge density in the plane through Hf_A, O_A, and O_i, and schematic diagram of doubly charged oxygen interstitial (O_i) near a threefold-coordinated oxygen (O_A) in hafnia. The charge density is in $0.1e/Å^3$ and all distances are in Å.

The changing nature of the defect pair can also be seen in the evolution of the total DOS of the systems. On addition of the neutral oxygen interstitial, the main band structure remains the same, but new states can be seen. These are bonding and antibonding states of the O_i-O_A defect pair due to the extensive charge transfer and formation of a strong covalent bond. The highest occupied defect states are in the band gap near the top of the valence band at 2.3 eV. The corresponding vertical hole affinities are equal to 0.12 eV, 0.30 eV, and 0.32 eV for the neutral and two charged defect pairs, correspondingly. For the singly charged oxygen interstitial, the O_i-O_A bond is weaker and the DOS is even closer to the ideal bulk DOS. The fact that the defect pair separates and becomes much more ionic means that there are now no other clear defect states in the DOS. Defect states appear at the top of the valence band in the gap at about 2.8 eV. The DOS for the doubly charged interstitial is, again, very similar to that for the perfect lattice, with O_i^{2-}-related defect states at about 2.7 eV in the gap.

IV. INCORPORATION OF MOLECULAR OXYGEN

Molecular oxygen species may incorporate into the hafnia lattice from the gas phase or form due to the interaction of

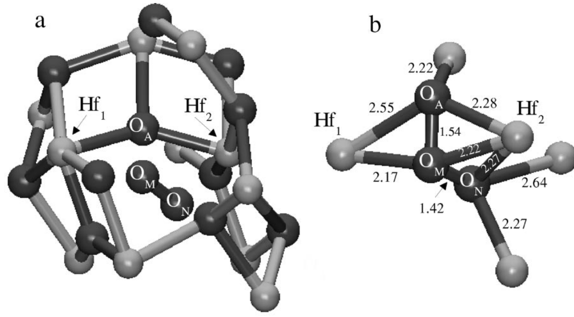

FIG. 6. (a) Atomic structure of ideal monoclinic hafnia with the neutral interstitial oxygen molecule (O_N-O_M) introduced near the threefold-coordinated lattice oxygen site (O_A). (b) Close-up of the defect structure after relaxation. Equivalent atoms in the ideal and defected structure are labeled. All distances are in Å.

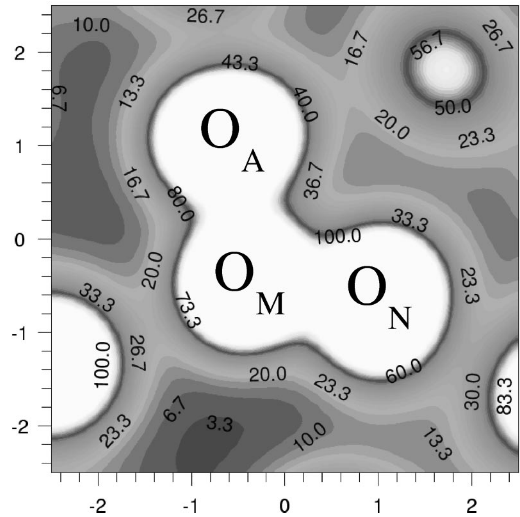

FIG. 7. Charge density of the neutral interstitial oxygen molecule (O_N-O_M) bonding with threefold-coordinated lattice oxygen site (O_A). The charge density is taken in a plane through O_M, O_N, and O_A in $0.1e/\text{Å}^3$ and all distances are in Å.

atomic oxygen species already existing inside the lattice. Direct analogy with silica in this case may be not extremely helpful, since there is much less space available in hafnia compared to, for example, quartz. To see whether the atomic or molecular form of oxygen incorporation is energetically favored we first consider incorporation of neutral oxygen molecules. Then extra electrons were again added into the system to study whether oxygen molecules can serve as electron traps.

A. Incorporation energies

Using Eq. (1) with E_{O_2} equal to 9.81 eV, we find incorporation energies of $+4.2$ eV for $(O_2^0)_3$ and $+5.8$ eV for $(O_2^0)_4$. As for the atomic case, incorporation near the less cramped threefold-coordinated oxygen lattice site is more favored. These molecular incorporation energies are double that found in silica,[43] as to be expected considering the greater interstitial space available in the silica lattice.

Comparison of atomic and molecular incorporation depends on the process by which the oxygen enters the system. If the process includes dissociation of the molecule, at a cost of 5.88 eV, we can compare the incorporation energy of a molecule in hafnia (4.2 eV) with the incorporation of two oxygen atoms (3.2 eV), implying that atomic incorporation is favored by only 1 eV. Again this contrasts with the favoring of molecular adsorption in silica by 2 eV.[43] However, if incorporation may occur effectively from an atomic gas, without dissociation, this reduces the incorporation energy of two separate atoms to -2.6 eV and favors atomic versus molecular incorporation by almost 7 eV. Although we performed full calculations for the $(O_2^x)_4$ series of defects, in every case the $(O_2^x)_3$ equivalent was lower in energy, so we will focus in detail only on that series.

B. Defect models and electron affinities

Figure 6 shows the atomic structure of a neutral oxygen molecule incorporated near to a threefold-coordinated lattice oxygen site, with Fig. 7 showing the associated charge density plot. It is immediately evident that the molecule shares an electron density with the lattice oxygen: there is a high electron density between O_A and O_M, and a bond length very close to the molecule O_M-O_N bond length. Atoms around the molecule displace away from the site to create more space in the crystal, but these relaxations decay rapidly to less than 0.1 Å beyond the immediate neighbors. As a consequence of these displacements all the Hf-O bond lengths are significantly longer than those in the ideal bulk crystal (see Fig. 2). In this configuration the molecule incorporates in the singlet state, and the triplet state is 0.5 eV higher in energy.

To study whether there are other stable configurations of a neutral molecule inside the hafnia lattice, we started the geometry optimization from initial configurations far from any oxygen sites. We have found that a stable minimum exists with bonding of the molecule only to hafnium ions; however, this state was 0.23 eV higher in energy. This result suggests that the molecule has a high electron affinity in the oxide, as it seeks the most abundant source of electrons in the system—lattice oxygen sites.

Adding an electron to the molecular defect produces a situation similar to that for the atomic oxygen defect. The electron localizes fully on the defect only after atomic relaxation. Figure 8 shows how the bond between the molecule and the threefold-coordinated lattice oxygen disappears. The molecule displaces away from the lattice oxygen and is now effectively bonded only to Hf ions. The intramolecular bond length remains the same as in the neutral case. The large relaxation energy of 2.67 eV from the neutral geometry for this defect reflects the strong reconstruction. The relaxed affinity to an electron from the bottom of the hafnia conduction band (see Table III) is positive and larger than that for atomic species.

Addition of a further electron continues the development of the oxygen molecule as an ionic species in the crystal. Figure 9 shows that the molecule moves further away from the lattice oxygen, which now returns to the almost ideal

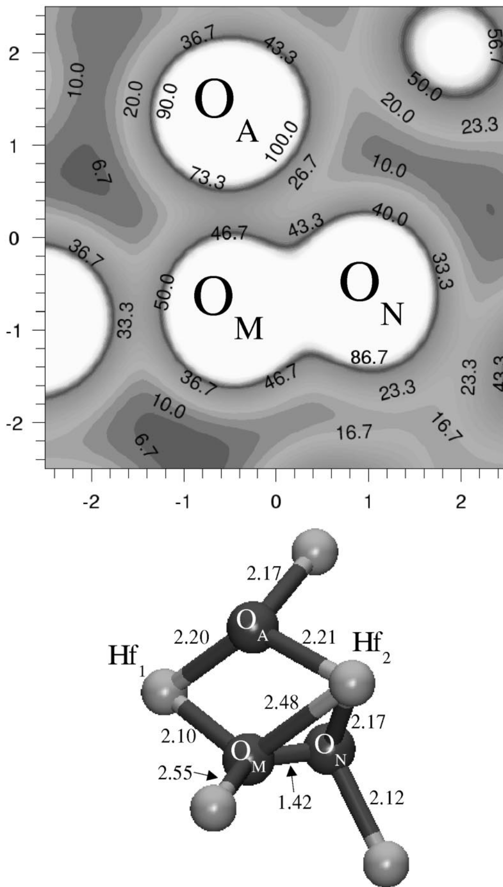

FIG. 8. Charge density and atomic structure of a singly charged interstitial oxygen molecule (O_N-O_M) near a threefold-coordinated lattice oxygen site (O_A). The charge density is taken in a plane through O_M, O_N, and O_A in $0.1e/\text{Å}^3$ and all distances are in Å.

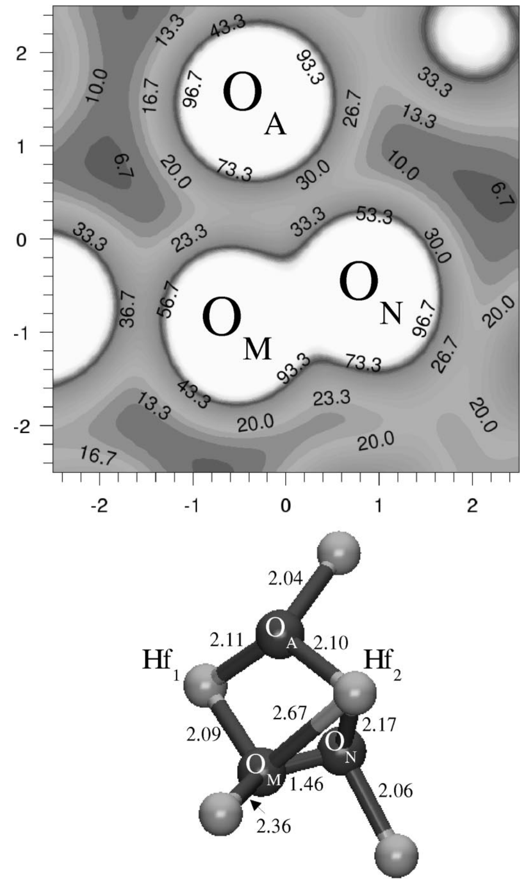

FIG. 9. Charge density and atomic structure of a doubly charged interstitial oxygen molecule (O_N-O_M) near a threefold-coordinated lattice oxygen site (O_A). The charge density is taken in a plane through O_M, O_N, and O_A in $0.1e/\text{Å}^3$ and all distances are in Å.

threefold-coordinated oxygen structure. The molecular bond length increases very slightly, but overall displacements are not very large. The relaxation energy from the singly charged geometry is 1.05 eV. The relaxed electron affinity of the molecule to the second electron from the bottom of the conduction band is again very large.

Figure 1(a) shows how the introduction of molecular defects to hafnia changes the total DOS. The incorporation of the neutral molecule produces several defect states due to the covalent bonds between the oxygens in the molecule and the lattice oxygen. Clear states due to charge transfer and the formation of covalent bonds between oxygen atoms can be seen at about −22 eV, −17 eV, −13 eV, −5 eV. As electrons are added to the system it tends towards the spectrum of the ideal bulk crystal. After an electron is added, the state at −17 eV disappears, and the other states decrease in energy and density, mirroring the dissipation of the covalent bond between O_A and O_M. A state now appears in the gap at 2.4 eV [see Fig. 1(b)]. The small hole affinities shown in Table III confirm that the states in the gap split from the valence edge when defects are introduced to the system. When a second electron is added only very small changes in the DOS can be observed, in agreement with the similar bonding seen around the molecule in both charged states.

V. OXYGEN AND HAFNIUM VACANCIES

Vacancies can be generated in hafnia films and bulk samples due to growth, deposition, and doping processes. In this section we will first focus on the structure and electronic properties of neutral oxygen and hafnium atom vacancies. In each case, the vacancy was initially generated by removing the corresponding neutral atom from its site in the relaxed perfect lattice supercell, followed by full atomic relaxation. Charged oxygen vacancies are also well known in many oxides, such as MgO and silica. Besides thermal processes and doping, they can be generated in thin hafnia films by electron and hole trapping from silicon. Once generated, they can take part in other electronic processes and serve as electron traps. Therefore we also consider the generation of charged vacancies by removal of electrons from the system.

Finally, it is interesting to study the effect of Zr ion substitution into the hafnia crystal. Due to their identical configuration of the outer electronic shell, hafnium and zirconium atoms display very similar properties. In fact, both types of atoms are often found together in natural minerals.[1] Also, since the Zr atom is slightly larger than Hf, there could be some similarity with Ge substitution for Si in SiO_2.[47,48]

A. Oxygen vacancies

We start our discussion with neutral oxygen vacancies. There are two types of oxygen vacancies in monoclinic hafnia: threefold- and fourfold-coordinated (V_3 and V_4, respectively). The lattice relaxation around them involves small displacements of the nearest-neighbor Hf ions. The displacements of these ions for both types of vacancies are in the range of 0.01–0.02 Å, which corresponds to 0.5–1.0% of the Hf-O bond length. These values are very similar to those obtained for oxygen vacancies in zirconia.[20] Such small displacements are characteristic for the *F*-center type defects well studied in cubic ionic oxides, such as MgO.[49,50] They correspond to almost full screening of the anion vacancy by the two remaining electrons, which are strongly localized around the vacancy site. The relaxation energies with respect to the perfect lattice are 0.09 eV and 0.06 eV for V_3 and V_4, respectively. Using Eq. (1), we obtain the vacancy formation energies of $E_{for}(V_3)=9.36$ eV and $E_{for}(V_4)=9.34$ eV, correspondingly. These values are also similar to those obtained for MgO,[49,50] silica,[49,51] and ZrO_2.[20] The formation of a vacancy introduces a new double-occupied one-electron level in the band gap situated at 2.8 eV and 2.3 eV above the top of the valence band for V_3 and V_4, respectively. Note that the corresponding vertical hole affinities are 2.4 eV and 1.8 eV.

One can estimate the vertical excitation energy of the vacancy into the lowest triplet excited state by calculating the singlet to triplet transition, $S_0 \rightarrow T_1$. Comparing the total energies of the supercells we obtain $E_{(S_0\rightarrow T_1)}(V_3)=1.30$ eV and $E_{(S_0\rightarrow T_1)}(V_4)=1.59$ eV, which are very similar to the values obtained by directly subtracting the energies of the one-electron states (1.22 eV for V_3 and 1.66 eV for V_4). We should note, however, that these excited states are delocalized at the bottom of the crystal conduction band. This may be due to the fact that the position of the bottom of the conduction band is too low in our DFT calculations. Localized defect excited states can be located below a proper conduction band, as is the case in, e.g., MgO.[52,53] Due to the same reason an extra electron added to the neutral vacancy appears to be delocalized at the bottom of the conduction band and the electron affinity of the neutral vacancy cannot be reliably established.

Removing an electron from the relaxed neutral vacancies results in formation of the positively charged defects, V_3^+ and V_4^+. The Hf ions surrounding the vacancy displace outwards by about 0.1–0.2 Å (5–10% of the Hf-O distance). This is much bigger than for the neutral vacancy. The relaxation energies are 0.65 eV and 0.61 eV for V_3^+ and V_4^+, respectively. The strong relaxation is caused by the fact that the neighboring Hf ions lose part of the screening effect provided by the two electrons in the neutral vacancy case. The remaining electron is strongly localized inside the vacancy site, as can be seen in the spin density map shown in Fig. 10. The vertical ionization energies for both types of neutral vacancies are given in Table III. The single-occupied one-electron state of this defect lies lower in the band gap. Its vertical hole affinity is 2.0 eV and 1.6 eV for V_3^+ and V_4^+, respectively. Vertical ionization energies given in Table III are correspondingly larger than for the neutral defect.

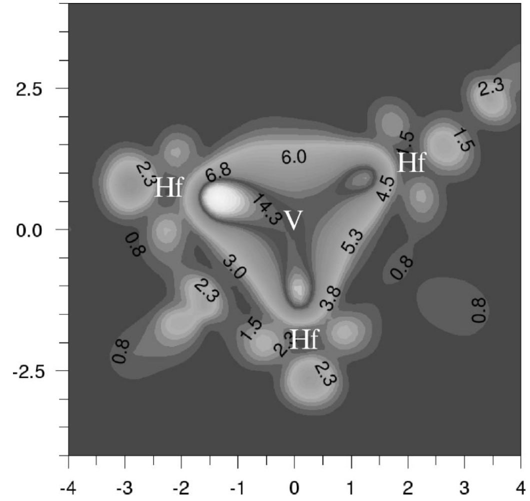

FIG. 10. Spin density in a plane containing three Hf ions neighboring the threefold-coordinated oxygen vacancy (*V*) with one electron removed from the system. The charge density is in $0.1e/\text{Å}^3$ and all distances are in Å.

Removal of yet another electron from the system leads to the formation of doubly positively charged vacancies, V_3^{2+} and V_4^{2+}. The Hf ions neighboring the vacancy site are displaced outwards by about 0.1–0.2 Å, and the relaxation energy is about 0.8 eV. Note that for both the V^+ and V^{2+}defects, the system total energy is much lower (0.44 eV and 0.76 eV, respectively) for the threefold-coordinated site. This implies that although formation of an initial neutral vacancy is energetically balanced between sites, once electrons are removed the V_3^X species is strongly favored and vacancies are likely to diffuse to these sites.

B. Hafnium vacancy

To complete this study we have also considered formation of a neutral Hf vacancy. The formation energy of this vacancy can be obtained using the expression $E_{for}(V_{Hf})=E_V+E_{Hf}-E_0^0$. Here, E_{Hf} can be calculated in two ways depending on the process being modeled. First, one can use a bulk metal reference state (once again avoiding the problems associated with calculating atoms in the periodic model), which gives $E_{Hf}=-9.88$ eV and $E_{for}(V_{Hf})=16.9$ eV. This would correspond to formation of Hf clusters in the bulk or at the surface of the oxide. However, one can also consider the situation where the removed hafnium remains always in equilibrium with oxygen vapor (see also discussion in Ref. 24). In this case it should be referenced with respect to the oxide. Then $E_{Hf}=E_{HfO_2}-E_{O_2}$, where E_{HfO_2} is the total energy per HfO_2 of monoclinic bulk hafnia and E_{O_2} is the total energy of the oxygen molecule. This method gives $E_{Hf}=-20.83$ eV and $E_{for}(V_{Hf})=5.7$ eV.

Creation of the Hf vacancy causes strong (up to 0.1–0.2 Å) outward displacements of the neighboring oxygen ions. The reason for such a strong relaxation is the repulsion felt by the oxygen ions as soon as the Hf atom is

removed. The presence of the Hf vacancy does not introduce any additional level in the gap.

C. Substitutional defects

We also considered substitution of one of the Hf atoms by a Zr atom in the relaxed perfect supercell, creating a substitutional zirconium defect, S_{Zr}. Due to similar electronic structure, the bonding established by the Zr ion is very close to the one by the Hf ion in the same site. Owing to the larger radius of Zr, there is, however, a small outwards relaxation of the oxygen atoms neighboring the Zr site. This is also consistent with the fact that the Zr-O distance in zirconia is bigger than the Hf-O distance in hafnia. These displacements are of the order of 0.01–0.02 Å. The presence of the Zr ion does not introduce any additional level in the band gap. If we consider the overall process of removal of a Hf atom followed by implantation of a Zr atom, then the formation energy can be defined,

$$E_{\mathrm{for}}(S_{\mathrm{Zr}})=E_{S_{\mathrm{Zr}}}+E_{\mathrm{Hf}}-E_{\mathrm{Zr}}-E_0^0,$$

where $E_{\mathrm{Hf}}=-3.36$ eV and $E_{\mathrm{Zr}}=-2.23$ eV. In this case $E_{\mathrm{for}}(S_{\mathrm{Zr}})$ is $+0.55$ eV using the bulk metal references for atomic energies and -0.05 eV for the oxide references. This means that some energy must be paid to exchange metal ions between bulk metal and oxide, but exchange between oxides is almost free—as to be expected for oxides with such similar properties.

Substitutional Ge defects in silica are known to be electron and hole traps.[48,54] To study whether the S_{Zr} defect in hafnia would exhibit similar properties we have considered charged systems by removing or adding one electron to the relaxed defect structure. However, both the extra hole and electron remained delocalized. This is consistent with the fact that Zr is very similar to Hf, and that the monoclinic hafnia lattice is much more compact than silica. Therefore charging of the substituted supercell presents qualitatively similar behavior as charging of the perfect cell. However, as has already been noted above, our DFT calculations are not capable of treating very shallow states. Therefore these results suggest that no deep electron and hole trapping states are induced by Zr substitution.

We have also studied the properties of a defect formed by a substitutional Zr atom and an adjacent oxygen vacancy, $S_{\mathrm{Zr}}+V_3$. It introduces a one-electron level in the band gap of hafnia at 2.7 eV above the top of the valence band, similar to the case of a single V_3 vacancy. In the neutral defect state this level is doubly occupied and the electrons remain strongly localized in the vacancy. The bigger substitutional Zr ion displaces towards the vacant site by about 0.08 Å. Some of the oxygen atoms in the vicinity of the vacancy cage move towards it, attracted by the Zr ion. The range of these displacements is 0.01–0.04 Å. Finally, some of the neighboring Hf ions move away from the defect site, with displacements of around 0.01 Å. The ions further away from the defect experience almost no relaxation. However, as one can see in Table III, this relaxation does not significantly affect the properties of the vacancy: the calculated ionization energies and electron affinities are very similar to those obtained for the single vacancy.

TABLE IV. Defect reactions and associated energies.

No.	Reaction	Energy (eV)
1	$O^0+V^0\Rightarrow O^-+V^+$	0.7
2	$O^-+V^+\Rightarrow O^{2-}+V^{2+}$	1.5
3	$O^{2-}+O^0\Rightarrow 2O^-$	−0.8
4	$V_4^{2+}+V_4^0\Rightarrow 2V_4^+$	0.0
5	$V_3^{2+}+V_3^0\Rightarrow 2V_3^+$	0.2
6	$O_2^0+V^0\Rightarrow O_2^-+V^+$	1.4
7	$O_2^-+V^+\Rightarrow O_2^{2-}+V^{2+}$	1.8
8	$O_2^{2-}+O_2^0\Rightarrow 2O_2^-$	−0.4
9	$2O^0\Rightarrow O_2^0+E_0^0$	−1.0
10	$O^0+O^-\Rightarrow O_2^-+E_0^0$	−0.3
11	$2O^-\Rightarrow O_2^{2-}+E_0^0$	0.8
12	$O_2^0+V^0\Rightarrow O^0+E_0^0$	9.0
13	$O_2^-+V^+\Rightarrow O^0+E_0^0$	7.6
14	$O_2^{2-}+V^{2+}\Rightarrow O^0+E_0^0$	5.7

VI. MODEL PROCESSES

The actual defects present in a real system will depend on the processing, electron source, applied voltage, and temperature of that system. However, assuming an initial distribution of defects in different charge states and electron transfer between defects, we can combine the obtained information about the various defects in different charge states to make some predictions about which defect combinations are energetically more favorable. We can also consider the defects levels with respect to the hafnia and silicon conduction bands; these may serve as an indication of electron and hole trapping in real devices.

A. Defect reactions

Various reactions and their energies are presented in Table IV. These energies have been calculated as differences in total energies of pairs of individual defects and each pair has the same total charge state and number of atoms. Positive energies indicate that a reaction in the direction of the arrow is energetically favorable. Note that we do not consider any reactions that include total energies with delocalized states, e.g., O^+ and V^-. The energies presented in Table IV also do not include the interaction between defects, which can be strong especially in close charged defect pairs.

Reactions 1 and 2 in Table IV indicate that charge transfer between oxygen vacancies and interstitials is favorable. A separated pair of doubly charged defects has 1.5 eV lower energy than the neutral pair. The associated Frenkel pair energies are 8.0 eV for formation of the neutral pair, 7.3 eV for the singly charged pair, and 5.8 eV for the doubly charged pair.

As for calculations of zirconia,[20] reaction 3 predicts "negative U" behavior of an oxygen ion in hafnia, i.e., that two isolated O^- species would decay into O^{2-} and O^0. The

same is true for molecular species but with a much smaller energy gain: reaction 8 shows that the oxygen molecule also has "negative U," and two O_2^- species would decay forming a doubly charged and a neutral molecule. This terminology comes from Anderson's model for semiconductors where this effect is much more common than in insulators.[55,56] Experimentally this means that atomic and molecular oxygen species in hafnia prefer to stay diamagnetic and will be difficult or impossible to detect using paramagnetic resonance. A similar process for vacancies in reaction 4 shows a balance between the different pairs for fourfold-coordinated and a slight energy gain of 0.2 eV for threefold-coordinated to form two singly charged vacancies. Again this is very similar to the results found in zirconia. However, in this case concentration of paramagnetic V^+ vacancies will strongly depend on temperature. Molecular species also demonstrate a tendency for charge transfer between the vacancies and interstitial molecules. The doubly charged molecule and vacancy pair is 3.2 eV lower in energy than the neutral pair (reactions 6 and 7).

Finally we study some reactions with respect to changes in the type of defect, rather than just the charge state. In these reactions we consider two independent defects combining to form a different defect, where the energy of the perfect lattice, E_0^0 [as in Eq. (1)], is included to conserve the number of particles. Here we see in reaction 9, as discussed previously, that it is energetically favorable for an oxygen molecule to separate into two interstitial atoms. However, two singly charged interstitial oxygen ions would like to recombine and form a doubly charged interstitial molecule (reaction 11). Also, we see that the calculations predict that all combinations of molecule and vacancy defect pairs (reactions 12–14) would "annihilate," leaving only a neutral oxygen interstitial. The energy gain is less for the more favorable doubly charged defect pair. These reactions are likely to take place during annealing of oxide in an oxygen atmosphere.

B. Electron and hole trapping

The calculated ionization energies and relaxed electron affinities of various defects are summarized in Table III. Large electron affinities clearly indicate that interstitial oxygen species and charged vacancies may serve as traps for electrons from hafnia conduction band. The calculated absolute values of relaxed hole affinities for charged oxygen species are large due to the strong defect relaxation. The "vertical" values for these affinities are about 0.3 eV, in line with what one would expect from the DOS and vertical ionization energies.

To facilitate further discussion, the electron affinities are also shown in a schematic energy diagram in Fig. 11, which can be used to estimate the electron affinities of these defects with respect to electrons from the bottom of silicon conduction band at the Si/HfO_2 interface. This is particularly relevant for thin oxide films where electrons can tunnel from the interface into defect states.[57] Counting from the top of the valence band of HfO_2 (see Fig. 11), we can use a theoretical estimate[58] of the valence band offset at the interface and the band gap of Si (1.1 eV) to estimate the energy of an

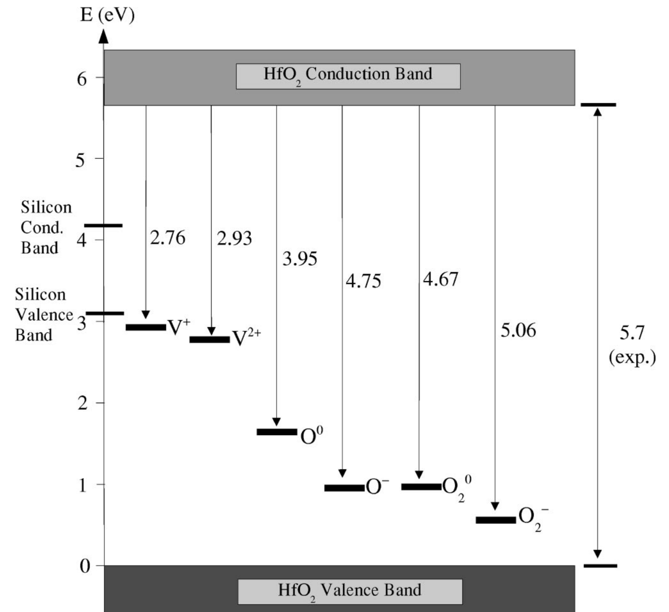

FIG. 11. Energy level diagram showing the electron affinities for various defects in monoclinic hafnia. All energies are in eV.

electron at the bottom of Si conduction band with respect to the defect levels. In all cases the relaxed electron states of defects are lower than the bottom of the bulk Si conduction band, suggesting the possibility of electron tunneling from Si. We should stress, however, that these results do not provide information regarding cross sections for electron/hole trapping on these defects; they only predict the energies gained by the process. Calculation of the probability of trapping requires a further study to determine the kinetics of electron/hole trapping.

Several other atomic and molecular charged defects were also studied in this work, specifically O_3^+, $(O_2^+)_3$, V_3^-, and V_4^-. However, each of these suffers from a limitation of the calculation method. The charge density maps of the relaxed structure show that the hole/electron is delocalized over the whole cell and the one-electron energy spectrum is typical for a metallic state. The relaxations of the ions are also much smaller than for the equivalent oppositely charged defect. This effect may represent an error in the kinetic energy calculated in Kohn-Sham theory, which favors delocalized over localized defect states,[44–46] and therefore these results were not discussed in detail.

VII. CONCLUSIONS

We have studied the structure of oxygen vacancy and interstitial defects in monoclinic hafnia and considered their ability to trap electrons and holes from the conduction and valence bands of hafnia. The results complement the results of previous similar works on zirconia[20] and zircon.[24] The qualitative defect models emerging from these studies are very similar to those found in other materials. In particular, oxygen vacancies in these materials have the structure and properties similar to those of F centers in cubic oxides (see also discussion in Ref. 59). Incorporation of atomic oxygen

species is more favorable than molecular ones. This result corroborates the experimental data on the isotope exchange of oxygen species in zirconia.[16] Structural models of atomic oxygen species calculated in silica[39] and O_2^- defects observed in MgO (Ref. 60) and SrO (Ref. 61) are qualitatively similar to those we find for hafnia: they bond with a lattice oxygen, forming a pair defect between two cations. Also in analogy with silica, charged atomic and molecular oxygen species tend to be more stable than neutral species when electrons are available from the bottom of the conduction band of hafnia.

The predicted possibility of electron transfer from silicon into oxygen vacancies and interstitials will have different consequences for the growth and annealing of hafnia films on silicon. In particular, electron transfer from silicon onto interstitial oxygen atoms creates charged oxygen ions, which will become attracted to or repelled from the interface by the image interaction with silicon dependent on which material has higher dielectric constant. This may affect diffusion of these species and thus the kinetics of oxide annealing and growth of silicon dioxide at the interface.[38] Existence of charged defects may also affect the reliability of devices as they create electric field, which may shift band offset, and produce dielectric losses. These problems certainly require a much more detailed study, including the mechanism of diffusion of charged oxygen species in hafnia.

ACKNOWLEDGMENTS

This research has been supported by the Academy of Finland through its Centres of Excellence Program (2000–2005). A.S.F. wishes to thank the Centre for Scientific Computing, Helsinki for use of its computational resources. A.L.S. is grateful to Fujitsu and the EU Framework5 HIKE project for financial support of this work. The authors wish to thank V. Afanas'ev, G. Bersuker, A. Korkin, N. Petrik, A. M. Stoneham, and A. M. Szymanski for useful discussions, and P. V. Sushko, V. B. Sulimov, and J. L. Gavartin for valuable comments on the manuscript. The LEV00 code[62] was used for calculation of density maps and DOS.

[1] J. Wang, H.P. Li, and R. Stevens, J. Mater. Sci. **27**, 5397 (1992).
[2] M. Balog, M. Schieber, M. Michiman, and S. Patai, Thin Solid Films **41**, 247 (1977).
[3] E. Ryshkewitch and D. W. Richerson, *Oxide Ceramics: Physical Chemistry and Technology* (Academic, Florida, 1985).
[4] A.J. Waldorf, J.A. Dobrowolski, B.T. Sullivan, and L.M. Plante, Appl. Opt. **32**, 5583 (1993).
[5] C.J. Howard, R.J. Hill, and B.E. Reichert, Acta Crystallogr., Sect. B: Struct. Sci. **44**, 116 (1988).
[6] R. Ruh and P.W.R. Corfield, J. Am. Ceram. Soc. **53**, 126 (1970).
[7] D.M. Adams, S. Leonard, D.R. Russel, and R.J. Cernik, J. Phys. Chem. Solids **52**, 1181 (1991).
[8] A. Lakhlifi, C. Leroux, P. Satre, B. Durand, M. Roubin, and G. Nihoul, J. Solid State Chem. **119**, 289 (1995).
[9] A.I. Kingon, J.P. Maria, and S.K. Streiffer, Nature (London) **406**, 1032 (2000).
[10] G.D. Wilk, R.M. Wallace, and J.M. Anthony, Appl. Phys. Lett. **74**, 2854 (1999).
[11] G.D. Wilk, R.M. Wallace, and J.M. Anthony, J. Appl. Phys. **87**, 484 (2000).
[12] B.H. Lee, L. Kang, R. Nieh, W.-J. Qi, and J.C. Lee, Appl. Phys. Lett. **76**, 1926 (2000).
[13] J. Aarik, A. Aidla, H. Mändar, V. Sammelsberg, and T. Uuustare, J. Cryst. Growth **220**, 105 (2000).
[14] D.A. Neumayer and E. Cartier, J. Appl. Phys. **90**, 1801 (2001).
[15] L. Koltunski and R.A.B. Devine, Appl. Phys. Lett. **79**, 320 (2001).
[16] B.W. Busch, W.H. Schulte, E. Garfunkel, T. Gustafsson, W. Qi, R. Nieh, and J. Lee, Phys. Rev. B **62**, R13 290 (2000).
[17] U. Brossman, R. Würschum, U. Södervall, and H.-E. Schaefer, J. Appl. Phys. **85**, 7646 (1999).
[18] D. Martin and D. Duprez, J. Phys. Chem. **100**, 9429 (1996).
[19] J.R. Chavez, R.A.B. Devine, and L. Koltunski, J. Appl. Phys. **90**, 4284 (2001).
[20] A.S. Foster, V.B. Sulimov, F.L. Gejo, A.L. Shluger, and R.M. Nieminen, Phys. Rev. B **64**, 224108 (2001).
[21] A. M. Stoneham, J. Non-Cryst. Solids (to be published).
[22] G. Stapper, M. Bernasconi, N. Nicoloso, and M. Parrinello, Phys. Rev. B **59**, 797 (1999).
[23] B. Králik, E.K. Chang, and S.G. Louie, Phys. Rev. B **57**, 7027 (1998).
[24] J.P. Crocombette, Phys. Chem. Miner. **27**, 138 (1999).
[25] W.B. Fowler, J.K. Rudra, M.E. Zvanut, and F.J. Feigl, Phys. Rev. B **41**, 8313 (1990).
[26] G. Kresse and J. Furthmüller, Comput. Mater. Sci. **6**, 15 (1996).
[27] G. Kresse and J. Furthmüller, Phys. Rev. B **54**, 11 169 (1996).
[28] J.P. Perdew, J.A. Chevary, S.H. Vosko, K.A. Jackson, M.R. Pederson, D.J. Singh, and C. Fiolhais, Phys. Rev. B **46**, 6671 (1992).
[29] D. Vanderbilt, Phys. Rev. B **41**, 7892 (1990).
[30] G. Kresse and J. Hafner, J. Phys.: Condens. Matter **6**, 8245 (1994).
[31] D. Murnaghan, Proc. Natl. Acad. Sci. U.S.A. **30**, 244 (1944).
[32] R. C. West, *Handbook of Chemistry and Physics* (CRC, Boca Raton, 1986).
[33] M. Winter, www.webelements.com
[34] D.W. Stacy, J.K. Johnstone, and D.R. Wilder, J. Am. Ceram. Soc. **55**, 482 (1972).
[35] A.A. Demkov, Phys. Status Solidi B **226**, 57 (2001).
[36] M. Leslie and M.J. Gillan, J. Phys. C **18**, 973 (1985).
[37] L.N. Kantorovich, Phys. Rev. B **60**, 15 476 (1999).
[38] A.M. Stoneham, M.A. Szymanski, and A.L. Shluger, Phys. Rev. B **63**, 241304 (2001).
[39] M.A. Szymanski, A.L. Shluger, and A.M. Stoneham, Phys. Rev. B **63**, 224207 (2001).
[40] S. Ramanathan, G.D. Wilk, D.A. Muller, C.M. Park, and P.C. McIntyre, Appl. Phys. Lett. **79**, 2621 (2001).
[41] D.R. Hamann, Phys. Rev. Lett. **81**, 3447 (1998).
[42] G. Pacchioni and G. Ieranò, Phys. Rev. B **56**, 7304 (1997).
[43] M.A. Szymanski, A.M. Stoneham, and A.L. Shluger, Solid-State Electron. **45**, 1233 (2001).

[44] J. Laegsgaard and K. Stokbro, Phys. Rev. Lett. **86**, 2834 (2001).
[45] J. L. Gavartin, P. V. Sushko, and A. L. Shluger, (unpublished).
[46] G. Pacchioni, F. Frigoli, D. Ricci, and J.A. Weil, Phys. Rev. B **63**, 054102 (2001).
[47] J.A. Weil, Phys. Chem. Miner. **10**, 149 (1984).
[48] V.B. Neustruev, J. Phys.: Condens. Matter **6**, 6901 (1994).
[49] G. Pacchioni, A.M. Ferrari, and G. Ieranò, Faraday Discuss. **106**, 155 (1997).
[50] L.N. Kantorovich, J.M. Holender, and M.J. Gillan, Surf. Sci. **343**, 221 (1997).
[51] V. B. Sulimov, P. V. Sushko, A. H. Edwards, A. L. Shluger, and A. M. Stoneham (unpublished).
[52] G.H. Rosenblatt, M.W. Rowe, G.P. Williams, R.T. Williams, and Y. Chen, Phys. Rev. B **39**, 10 309 (1989).
[53] Q.S. Wang and N.A.W. Holzwarth, Phys. Rev. B **41**, 3211 (1990).
[54] W. Hayes and T.J.L. Jenkin, J. Phys. C **19**, 6211 (1986).
[55] P.W. Anderson, Phys. Rev. Lett. **34**, 953 (1975).
[56] A.M. Stoneham and M.J.L. Sangster, Radiat. Eff. **73**, 267 (1983).
[57] W.B. Fowler, J.K. Rudra, M.E. Zvanut, and F.J. Feigl, Phys. Rev. B **41**, 8313 (1990).
[58] J. Robertson, J. Vac. Sci. Technol. B **18**, 1785 (2000).
[59] A.V. Emeline, A.V. Rudakova, V.K. Ryabchuk, and N. Serpone, J. Phys. Chem. B **102**, 10 906 (1998).
[60] L.E. Halliburton and L.A. Kappers, Solid State Commun. **26**, 111 (1978).
[61] V. Seeman, S. Reifman, T. Lehto, and U. Haldre, Phys. Status Solidi B **102**, 459 (1980).
[62] L. N. Kantorovich, www.cmmp.ucl.ac.uk/~lev/codes/lev00/index.html